Applied Catalysis B: Environmental 288 (2021) 119997

Contents lists available at ScienceDirect

Applied Catalysis B: Environmental

journal homepage: www.elsevier.com/locate/apcatb

Synergistic effects altering reaction pathways: The case of glucose hydrogenation over Fe-Ni catalysts

Yang Fu [a], Lipeng Ding [b,c], Michael L. Singleton [a], Hosni Idrissi [b,c], Sophie Hermans [a,*]

[a] IMCN Institute, MOST Division, UCLouvain, 1 Place Louis Pasteur, B-1348 Louvain-la-Neuve, Belgium
[b] Institute of Mechanics, Materials and Civil Engineering, IMAP Division, UCLouvain, Place Sainte Barbe, 2, B-1348, Louvain-la-Neuve, Belgium
[c] Department of Physics, Electron Microscopy for Materials Science (EMAT), University of Antwerp, Groenenborgerlaan 171, 2020, Antwerpen, Belgium

ARTICLE INFO

Keywords:
Glucose hydrogenation
Non-noble metal
Synergistic effect
Nanoalloy

ABSTRACT

Carbon black (CB) supported Ni, Fe, or Fe-Ni alloy catalysts were synthesized by sol-gel to elucidate the reaction pathways over each catalyst, as well as synergistic effects in glucose to sorbitol hydrogenation. The bimetallic materials presented small and alloyed nanoparticles that were richer in reduced metallic sites at the surface than their monometallic counterparts. Glucose isomerization to fructose was favoured over Fe/CB, while glucose hydrogenation to sorbitol is the dominating pathway over Ni/CB catalyst. By contrast, sorbitol production was promoted and undesired isomerization was suppressed when Fe and Ni formed a nanoalloy. In addition, the alloy catalyst presented better stability than the corresponding monometallic catalyst. A comparison with a mechanical mixture of Fe/CB and Ni/CB monometallic catalysts demonstrated the synergy at the nanoscale in the alloy. By comparing different Fe:Ni ratios, the 1:1 formulation was identified as the best compromise to achieve a high activity while maintaining high sorbitol selectivity.

1. Introduction

Sorbitol was identified by the U.S. Department of Energy as one of the 12 most important value-added chemicals obtainable from biomass. It can be potentially used as a source of alkanes for liquid biofuels or as an "outstanding building block" for commodity chemicals [1,2]. Industrially, sorbitol is produced either via biochemical methods, such as conventional fermentation by *Zymomonas mobilis* or by chemical routes such as catalytic hydrogenation of glucose. Compared with fermentation processes, chemical approaches can be potentially more easily fine-tuned and refined to give higher production at lower costs. Notably, catalytic methods for obtaining sorbitol have attracted substantial attention recently.

The reduction of glucose to sorbitol by hydrogenation was first reported by Ipatieff and co-workers using a nickel catalyst at high temperature and pressure [3]. Based on kinetic studies, the reaction was found to be first order in glucose concentration and catalyst concentration, and half-order with respect to hydrogen pressure when using Raney nickel [4]. Wisnlak et al. also found that this reaction followed a similar pseudo-first-order course when using different catalysts or supported catalysts, such as ruthenium or rhodium supported by active carbon [5]. A challenging aspect of this hydrogenation is that side reactions involving epimerization of the substrate can occur, leading to lower yields or necessitating additional purification steps. While this problem is largely avoided by the use of noble metal catalysts, their cost has still largely limited their applicability for industrial processes. The less expensive nickel has been reported to show minimal epimerization, but generally has lower reactivity than Ru or Pt [6]. For this reason, increased interest has been placed on the development of new catalytic systems for improving the reactivity of base metals for the hydrogenation of glucose.

In the view of creating a higher number of catalytic sites with same amount of metal, nanoparticles, especially supported nanoparticles for glucose hydrogenation, have been broadly studied recently [7–9]. For example, the activity of SiO_2 supported amorphous Ni-B catalysts was reported to be adjusted by calcination temperature [10]. Schimpf and co-workers confirmed the necessity of complete reduction of precursors within Ni/SiO_2 catalyst to optimize activity and selectivity [7]. Besides SiO_2, other different supports like MWNTs (multi-walled carbon nanotubes), Al_2O_3, or TiO_2 were also applied to investigate the catalytic activities in this reaction, because different metal-support interactions could affect the activity and stability of metal particles [11–13]. For example, the Ru/MWNTs material showed the highest catalytic activity, compared with Raney Ni and ruthenium supported on Al_2O_3 or SiO_2

* Corresponding Author
E-mail addresses: yang.fu@uclouvain.be (Y. Fu), sophie.hermans@uclouvain.be (S. Hermans).

https://doi.org/10.1016/j.apcatb.2021.119997
Received 13 November 2020; Received in revised form 10 February 2021; Accepted 11 February 2021
Available online 16 February 2021
0926-3373/© 2021 Elsevier B.V. All rights reserved.

[14]. Ni catalysts supported on carbon were found to leach less compared with other Al_2O_3, TiO_2 or SiO_2 supports [13]. Additionally, carbon is robust at high pressure and temperature in aqueous solution. Thus, carbon is an ideal material to support metals with the desired catalyst activity and stability for glucose hydrogenation.

Regarding the metal, it is practical to find strategies to improve the activity of Ni-based catalysts as most commercial processes are still using Raney nickel [15]. Raney nickel has been reported to be enhanced by promoters like molybdenum, chromium, and iron [5,16,17]. Among them, Fe is the most electropositive metal and the glucose hydrogenation reaction with Fe promoted Raney Nickel catalyst exhibits the highest initial rate [18]. So, Fe as a promoter can maximally enhance the activity of Ni catalysts. Also, the magnetic properties of Fe make it easy to separate from the products for successive use when considering recycling. Since most of the previous works on this bimetallic association were focusing on the activity enhancement by an Fe promotor on Raney nickel [16,18], to the best of our knowledge, supported Ni-Fe-based catalysts have never been reported in the hydrogenation of glucose, let alone used to investigate the reaction pathways. Thus, Ni integrating Fe on carbon support catalysts is worth studying not only for fundamental research but also for industrial applications.

With this aim in mind, we synthesized Fe_xNi_y alloy catalysts, using carbon black (CB) as a support to study both their catalytic performance and the function of Fe and Ni atoms during the hydrogenation reaction. Moreover, the synergy and reaction pathway were also clarified. The catalytic transformation of glucose to sorbitol in the aqueous phase can be described as schematized in Fig. 1. The open-chain glucose conformer, transformed from the glucopyranose ring, is adsorbed on the FeNi alloy surface via the oxygen lone pairs. Then the polarization of the C═O bond favours nucleophilic addition of hydrides (H adatoms) present on the metal surface, producing sorbitol.

2. Experimental

2.1. Chemicals and materials

Nickel(II) nitrate hexahydrate [$Ni(NO_3)_2{\cdot}6H_2O$, 99.999 %, Sigma-Aldrich], iron(III) nitrate nonahydrate [$Fe(NO_3)_3{\cdot}9H_2O$, >98 %, Sigma-Aldrich], carbon black support [received as 250 G type from IMERYS GRAPHITE & CARBON], citric acid [$C_6H_8O_7$, 99.5 %, Alfa Aesar], and ethanol [C_2H_5OH, 100 %, Merck] were used as received.

2.2. Catalysts preparation

Synthesis of monometallic Fe/CB, Ni/CB catalysts.

The synthesis of Fe or Ni nanoparticles supported by carbon black was inspired by a Pechini-type sol-gel method [19]. In a typical procedure, 100 mg of CB, 400 mg of citric acid and 0.34−0.35 moles of the $M(NO_3)_n{\cdot}XH_2O$ salt (99.1 mg of $Ni(NO_3)_2{\cdot}6H_2O$ or 144.7 mg of $Fe(NO_3)_3{\cdot}9H_2O$) were added into a round-bottom flask equipped with a stir bar. After that, 6 ml of ethanol was added, and the mixture was stirred and sonicated until a homogenous suspension was obtained. Then, the suspension was heated at 90 °C for 3 h under reflux. Afterwards, the suspension was transferred into a ceramic boat and dried under vacuum at 30 °C until a gel formed. Finally, the gel was introduced in a tubular furnace and heated to 750 °C for 2 h under Ar/H_2 atmosphere. It should be stated that this temperature is sufficient to reduce nickel and iron precursors in monometallic and alloy samples [20]. The recovered magnetic powder was used as catalyst without further precautions.

Synthesis of Fe_3Ni/CB, FeNi/CB, $FeNi_3$/CB alloy catalysts.

The alloy catalysts were prepared following the same procedure as for the synthesis of monometallic Fe/CB (Ni/CB) detailed above, but with simultaneous addition of two metal salts in the following ratios: briefly, 24.8 mg of $Ni(NO_3)_2{\cdot}6H_2O$ and 108.5 mg of $Fe(NO_3)_3{\cdot}9H_2O$ were used to obtain the Fe_3Ni/CB catalyst. 49.6 mg of $Ni(NO_3)_2{\cdot}6H_2O$ and 72.3 mg of $Fe(NO_3)_3{\cdot}9H_2O$ were used to obtain FeNi/CB catalyst, and 74.3 mg of $Ni(NO_3)_2{\cdot}6H_2O$ and 36.2 mg of $Fe(NO_3)_3{\cdot}9H_2O$ were used to obtain the $FeNi_3$/CB catalyst.

2.3. Characterization

TEM images were obtained on a LEO 922 Omega Energy Filter Transmission Electron Microscope operating at 120 kV. TEM high angle annular dark field (HAADF) images and TEM-EDX elemental maps were obtained on a field emission gun (FEI) Osiris TEM operated at 200 kV equipped with a CHEMISTEM detector. The samples were suspended in ethanol under ultrasonic treatment. Three drops of the suspension were deposited on a holey carbon film supported on a copper grid (Holey Carbon Film 300 Mesh Cu).

X-ray photoelectron spectroscopy (XPS) analyses were carried out at room temperature with a SSI-X-probe (SSX 100/206) photoelectron spectrometer from Surface Science Instruments (USA), equipped with a monochromatized microfocus Al X-ray source (1486.6 eV). Samples

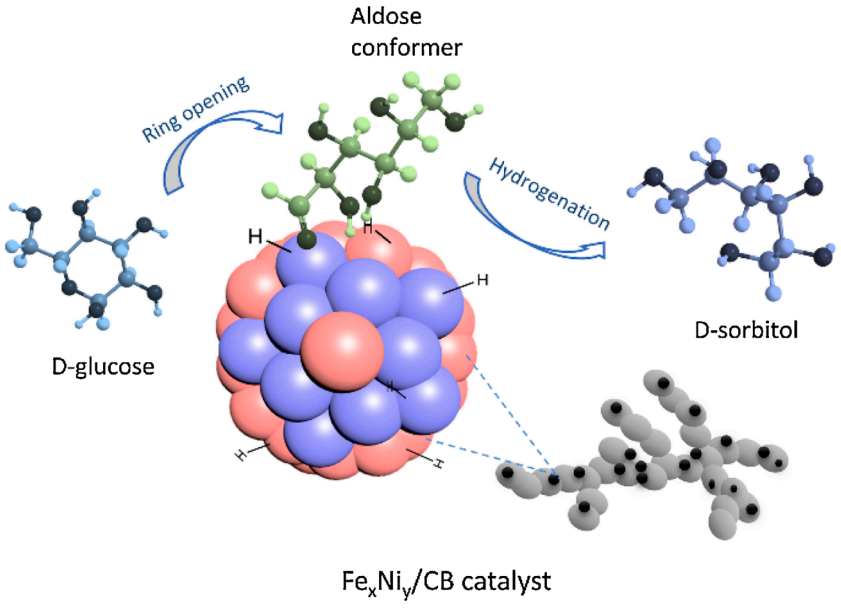


Fig. 1. Aqueous-phase hydrogenation of glucose to sorbitol on the surface of Fe_xNi_y alloy catalysts supported on carbon black.

were set on the sample holders by double face adhesive tape. Charging effect of the samples were eliminated by placing a nickel grid above the samples and using a flood gun set at 8 eV. All the binding energies were calculated according to the C-(C, H) component of the C 1s peak fixed at 284.4 eV. Data analysis was carried out using CasaXPS software, and the peaks were decomposed by Gaussian/Lorentzian product formula GL (15) after a Shirley-type background was subtracted.

For crystal phase identification, the powder sample was tiled on a silicon crystal sample holder, and its X-ray diffraction (XRD) analysis was conducted with a D8-Advance diffractometer (Bruker, Germany). The reference database PDF-2 2004 was launched to match experimental peaks.

The elemental analyses of solid carbon-based materials was determined by microgravimetry (weight loss associated with carbon calcination), and the elemental analyses of Fe and Ni were carried out by an ICAP 6500 thermoscientific spectrophotometer after acid digestion.

The specific surface area of the catalysts was measured through nitrogen adsorption-desorption isotherms, which was performed in a Micromeritics ASAP 2020 analyser at 77 K. Before analysis, the samples (around 0.2 g) were degassed for 2 h at 473 K with a heating rate of 10 K/min under 0.133 Pa pressure. The specific surface areas were calculated based on the Brunauer-Emmett-Teller (BET) equation by analysis of the isotherms.

2.4. Hydrogenation of D-glucose

Hydrogenation experiments were performed in a stainless-steel high pressure reactor (Parr autoclave) under the given conditions, typically, 140 °C at 30 bar H_2 using a stirring rate of 1700 rpm (which was sufficient to eliminate external mass-transport limitations) using 0.5 g of glucose and 60 mg of catalyst in 100 ml Milli-Q water. In brief, 60 mg of catalyst was added to the aqueous glucose solution, then the reactor was purged with N_2 for 5 min to remove air. The reaction mixture was subsequently heated to 140 °C under N_2, then the autoclave was filled to a constant H_2 pressure (30 bar) and the reaction started. For the kinetic tests, samples were periodically withdraw from the reaction vessel to evaluate the evolution with time of both glucose conversion and products yields. When single experiment ended, the filtrate of the reaction slurry was analysed by HPLC. HPLC analysis was performed on a Waters system equipped with a refractive index 2414 detector. An HPX-87C carbohydrate column was used, with ultrapure water as mobile phase at a flow rate of 0.5 $cm^3\ min^{-1}$, a column temperature of 358 K and 25 µl of injected volume. Standard alpha-D(+)-glucose ($C_6H_{12}O_6$, ≥ 99 %, Acros), D-(-)-fructose ($C_6H_{12}O_6$, ≥ 99 %, Sigma), D-(+)-mannose ($C_6H_{12}O_6$, ≥ 99 %, Sigma), D-mannitol ($C_6H_{14}O_6$, ≥ 98 %, Sigma-aldrich) and D-sorbitol ($C_6H_{14}O_6$, ≥ 99.5 %, Sigma) were first analysed by HPLC to determine their retention times separately, which were used as references to identify the products of glucose hydrogenation. The glucose conversion, sorbitol selectivity, product percentage yield and carbon balance (C_b) were calculated according to Eqs. 1–4:

$$\text{Conversion}(\%) = \frac{\text{moles of glucose (t = 0)} - \text{moles of glucose (t = i)}}{\text{moles of glucose (t = 0)}} \times 100 \quad (1)$$

$$\text{Selectivity}\ (\%) = \frac{\text{moles of sorbitol (t = i)}}{\text{moles of glucose(t = 0)} - \text{moles of glucose (t = i)}} \times 100 \quad (2)$$

$$\text{Yield}\ (\%) = \frac{\text{moles of product (t = i)}}{\text{moles of glucose (t = 0)}} \times 100 \quad (3)$$

$$C_b(\%) = \frac{n_{\text{glucose (t=i)}} + n_{\text{fructose}} + n_{\text{mannose}} + n_{\text{mannitol}} + n_{\text{sorbitol}}}{n_{\text{glucose (t=0)}}} \times 100 \quad (4)$$

3. Results and discussion

3.1. Characterization of Fe_xNi_y/CB catalysts

Three bimetallic Fe_xNi_y catalysts supported on carbon black, with different ratios between the two metals, were prepared. For comparison, monometallic materials were also synthesized by the same method. P-XRD was applied to determine the crystal phases in the synthesized nanocatalysts, and the patterns of the Fe_xNi_y/CB, Ni/CB, Fe/CB, as well as pure CB (black curve) are shown in Fig. 2. In each curve, one main broad peak at 2θ = 25.31° attributable to the (002) plane of graphite was observed along with a small hump at 2θ = 43.36° corresponding to the (100) plane (JCPDS-ICDD card No.41–1487), which revealed the disordered graphitic nature of CB. The peaks attributable to Fe, Ni, or FeNi phases were much stronger and sharper than those of carbon black, indicating the high crystallinity of the metal nanoparticles. The peaks at 2θ = 44.75° and 65.05° for Fe/CB corresponded to the (110) and (200) planes of crystalline body centered cubic (bcc) iron structure, respectively. The peaks at 2θ values of 44.51°, 51.83°, 76.37° corresponded to the (111), (200) and (220) crystal planes of crystalline face centered cubic (fcc) nickel in the Ni/CB catalyst, respectively. For bimetallic FeNi/CB catalyst with atomic ratio 1:1, the peaks at 2θ = 43.79°, 51.01°, 75.05° corresponded to the (111), (200) and (220) crystal planes of crystalline fcc FeNi alloy (JCPDS 12-0736). Each crystalline peak in FeNi/CB has shifted to the left compared to Ni/CB although they are both fcc phases, because the unit cell parameters increased when the larger Fe atoms entered the fcc structure of Ni. The XRD patterns of the two other Fe-Ni alloy catalysts supported on CB, namely Fe_3Ni/CB and $FeNi_3$/CB, with atomic ratios of 3:1 and 1:3, with a total metal loading unchanged around 16 wt% (theoretically), are also illustrated in Fig. 2. For Fe_3Ni/CB, the bcc and fcc phases coexisted in the alloy particles. The peaks at 2θ = 44.64°, 65.15° corresponded to the (110) and (200) planes of crystalline bcc Fe-Ni alloy structure (JCPDS37-0474), respectively. For $FeNi_3$/CB, the peaks at 2θ values of 44.16°, 51.44°, 75.71° corresponded to the (111), (200) and (220) crystal planes of crystalline fcc Fe-Ni alloy structure (JCPDS38-0419), respectively [21]. The average sizes of alloy nanoparticles that were calculated using the Debye–Scherrer formula based on the full-width at half-maximum (FWHM) of the (200) diffraction peak were 9.4 nm, 9.0 nm and 11.1 nm for $FeNi_3$/CB, FeNi/CB, and Fe_3Ni/CB materials, respectively.

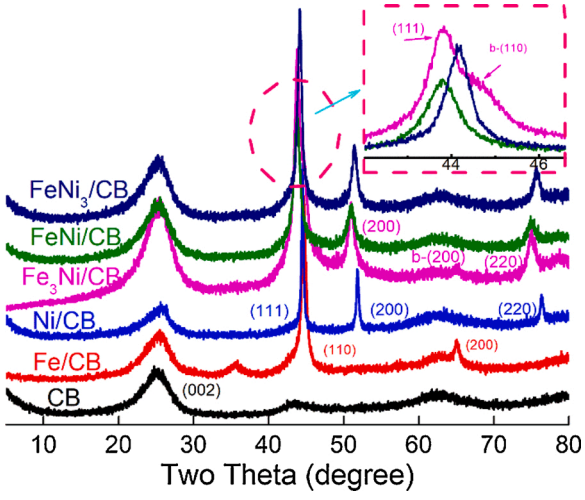


Fig. 2. Powder X-ray diffraction patterns of CB, Fe/CB, Ni/CB, Fe_3Ni/CB, FeNi/CB, $FeNi_3$/CB. Inserted imaged: the enlarged peaks around 2θ = 44° of Fe_3Ni/CB, FeNi/CB, $FeNi_3$/CB samples.

The STEM-HAADF images in Fig. 3a-c show that the as-prepared alloy catalysts exhibit mostly spherical morphology with a narrow size distribution (Fig. 3d-e), which is consistent with P-XRD analysis. Furthermore, the average nanoparticles size in Fe_3Ni/CB, FeNi/CB, $FeNi_3$/CB samples is almost the same, so the effect of particle sizes on catalytic performance can be eliminated. Meanwhile, STEM-EDX analysis (Figure S1 and Table S1) illustrated that the composition of the particles was stable from one to another, that is to say no monometallic Fe particles or Ni particles were observed in the bimetallic catalysts.

The metal loadings measured by ICP-OES are given in Table 1. These are slightly lower than theoretical values (based on engaged amounts). This is due to traces of insoluble ash during the digestion process causing systematic underestimation by ICP. However, those differences do not affect the comparison of the catalyst series with various compositions.

To study the textual properties of catalysts, adsorption/desorption isotherms of N_2 at −196 °C were determined and results are illustrated in Figure S2. The expected Type II isotherm was obtained for all the samples, which exhibit nonporous or macroporous texture, but the BET surface area showed differences among parent CB, monometallic catalysts and bimetallic catalysts (Table 1). The increase in BET surface area after nanoparticle loading is possibly due to nanoparticles anchored on the surface of CB, which provided the additional surface. It should be noted that those nonporous materials and exposed metal particles remain fully accessible to reactants.

The state and the occurrence of the different elements at the surface of the materials was evaluated through XPS. Fig. 4 illustrates the XPS spectra of the Ni $2p_{3/2}$ and Fe $2p_{3/2}$ region of Fe/CB, Ni/CB and FeNi/CB catalysts. The binding energies around 707 eV and 852 eV (red components) are ascribed to metallic Fe (Fe°) and metallic Ni (Ni°), respectively [22]. The peaks (blue components) around 710 eV and 854 eV are assigned to oxidized Fe ($Fe^{\delta+}$) and oxidized Ni ($Ni^{\delta+}$), along with two satellite peaks (pink peaks) [22]. The Ni (δ+) $2p_{3/2}$ peak (856.8 eV) of Ni/CB shifted towards lower binding energies with the introduction of Fe, while the Fe (δ+) $2p_{3/2}$ peak (706.79 eV) of Fe/CB moved towards higher binding energies after alloy formation with Ni. This shift of the binding energies may be attributed to partial electronic transfer from Fe to Ni in the FeNi/CB alloy catalysts [23,24]. Since the catalysts were stored with no particular precautions, an external Ni or Fe oxide layer could be formed due to contact with air, which explains the presence of oxidized Ni and Fe. It could be observed that there is no Ni° on the surface of the monometallic Ni/CB catalyst (Fig. 4b), while 22 % of Ni° exists in the FeNi/CB catalyst, and the metallic portions are even higher in the two other alloys (Table 2). As for Fe°, the proportion in the alloy catalysts is more than 2 times higher than it is in the monometallic Fe/CB catalyst. This suggests that a stabilization effect exists in the alloy catalysts, which could inhibit surface oxidation to some extent. As hydrogen is dissociated by the metallic atoms on the surface of the catalyst during the hydrogenation reaction [25], this remaining metallic Fe and Ni in the alloy catalysts are active sites, which can allow reaction without prereduction of the oxidation layer. From the comparison of XPS and ICP elemental analysis results (Table 2), it can be seen that those Fe:Ni ratios are almost the same, which mirrors the consistent internal and external compositions.

Table 1
Metal loading, Fe:Ni ratio, textural properties of Fe/CB, Ni/CB, Fe_3Ni/CB, FeNi/CB, $FeNi_3$/CB catalysts and bare CB support.

Catalyst	Fe	Ni	Fe:Ni	Fe	Ni	Fe:Ni	S_{BET} ($m^2\ g^{-1}$)
	Theoretical metal loading (wt%)			Measured metal loading (wt%) – ICP-OES			
CB	–	–	–	–	–	–	68.8
Fe/CB	14.29	–	–	11.1	–	–	141.2
Ni/CB	–	14.29	–	–	14.0	–	91.7
Fe_3Ni/CB	12.50	4.17	3.0	12.04	4.12	2.92	110.6
FeNi/CB	8.33	8.33	1.0	8.2	8.2	1	113.2
$FeNi_3$/CB	4.17	12.50	0.3	4.12	12.43	0.33	114.1

3.2. Activity test: hydrogenation of glucose

Catalytic hydrogenation of glucose in aqueous solution was employed as a model reaction to evaluate the catalytic performance. The reaction network and key products are illustrated in Fig. 5. As it is well known, sorbitol, one of the main hydrogenation products (pathway I), can be obtained from the open chain form of glucose, which only exists

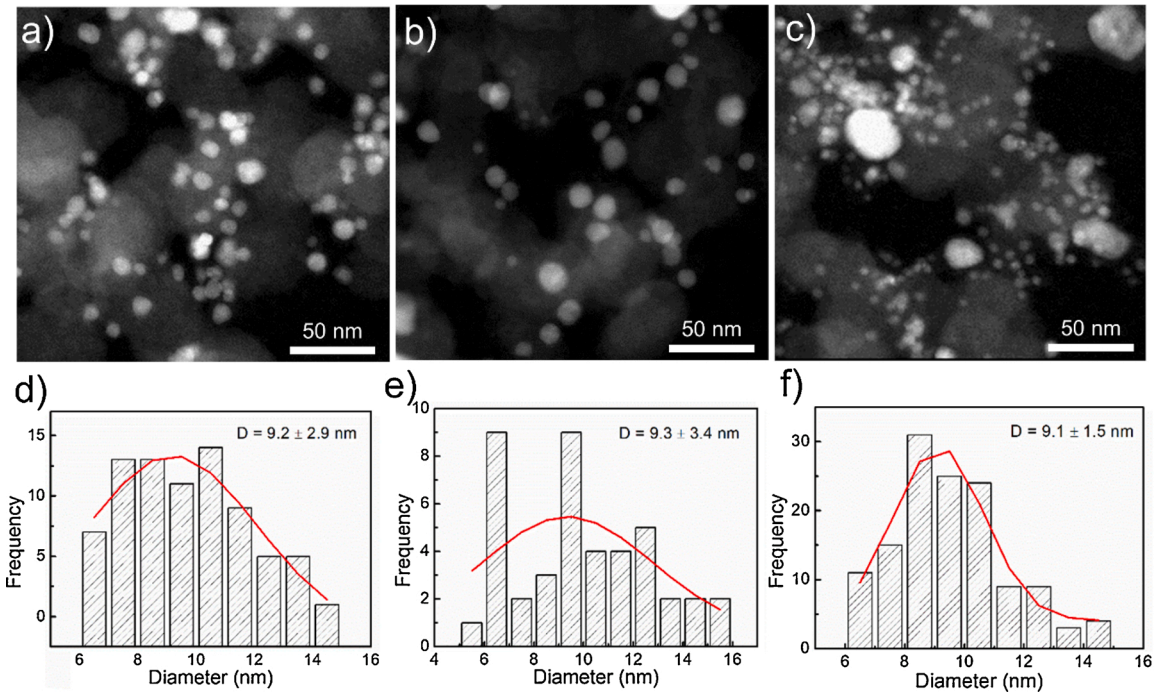


Fig. 3. STEM-HAADF images and nanoparticle size distributions determined with ImageJ software of Fe_3Ni/CB catalyst (a, d), FeNi/CB catalyst (b, e), and $FeNi_3$/CB catalyst (c, f).

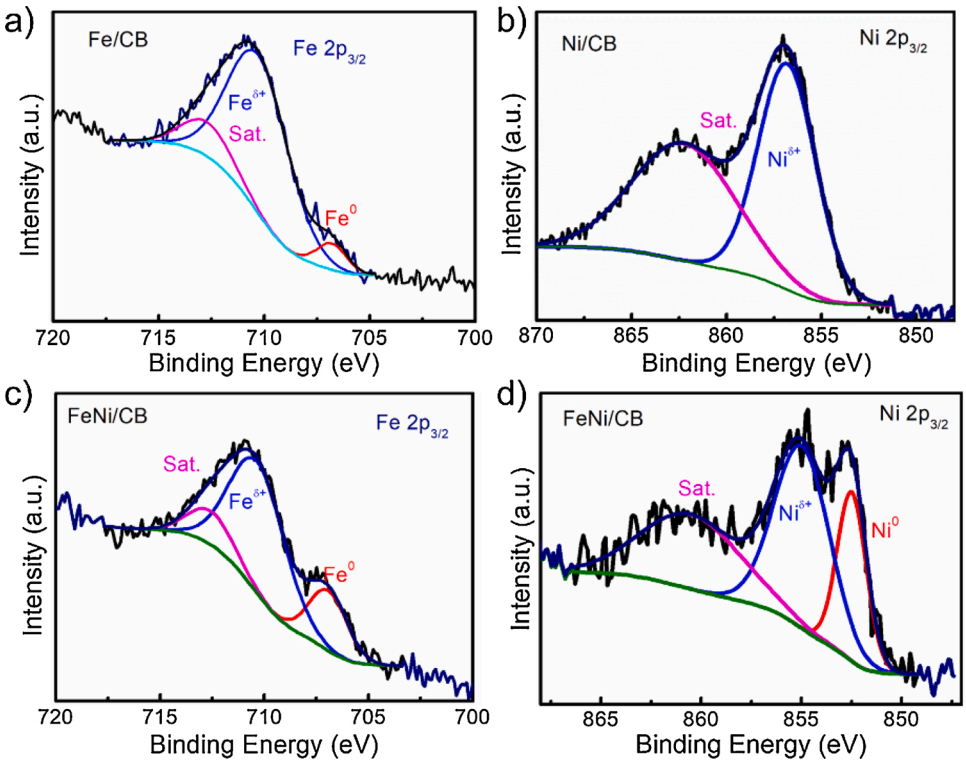


Fig. 4. Fitted Fe $2p_{3/2}$ and Ni $2p_{3/2}$ XPS spectra of (a) Ni/CB, (b) Fe/CB, (c, d) FeNi/CB catalysts. Fe (0), Ni (0) = red components; $Fe^{\delta+}$, $Ni^{\delta+}$ = blue components.

Table 2
Binding energy and contents in Fe^0, $Fe^{\delta+}$ in Fe $2p_{3/2}$ level and Ni^0, $Ni^{\delta+}$ in Ni $2p_{3/2}$ level; weight ratio of Fe and Ni obtained by XPS and ICP.

Catalyst	Fe^0 $2p_{3/2}$		$Fe^{\delta+}$ $2p_{3/2}$		Ni^0 $2p_{3/2}$		$Ni^{\delta+}$ $2p_{3/2}$		Fe:Ni (wt%)	
	B.E. (eV)	at.%	B.E. (eV)	at.%	B.E. (eV)	at.%	B.E. (eV)	at.%	XPS*	ICP
Fe/CB	706.79	6.5	710.26	93.5	–	–	–	–	–	–
Ni/CB	–	–	–	–	0	0.00	856.8	100.0	–	–
Fe_3Ni/CB	706.95	51.2	710.67	48.8	852.29	57.4	854.15	42.6	3.02 ± 0.3	2.92
FeNi/CB	706.93	20.8	710.3	79.2	852.49	22.0	854.97	78.0	0.92 ± 0.3	1
$FeNi_3$/CB	706.95	40.4	710.67	59.6	852.29	38.3	854.15	61.7	0.56 ± 0.3	0.33

* Atomic percentages have been converted into mass percentages.

at ~0.0026 mol% in solution due to its thermodynamic instability and its spontaneous isomerization to cyclic forms [26]. This open chain form then adsorbs on the metal surface via its O lone pair and subsequently gets reduced by the hydridic adatoms formed on the metal surface by H_2 splitting. Therefore, the formation of the open-chain conformation is generally considered to be the rate-limiting step [27]. Pathway II is glucose conversion to fructose, which involves the isomerization of an α-hydroxy aldehyde to the corresponding α-hydroxy ketone [28,29]. In the presence of catalytic Lewis acids, this process has been shown to occur via an intramolecular hydride shift. For the Fe/Ni catalysts, the isomerization could be catalysed by leached metal ions like Fe^{3+}, Ni^{2+} which would act as Lewis acids or also simply by metallic Fe [30]. The reversibility of this intramolecular process can also lead to epimerization of the C2 position and formation of mannose (pathway III) [31,32]. Mannitol in consequence would then be produced through fructose and mannose hydrogenation (IV, VI). As sorbitol, fructose, mannose and mannitol are the major products/reactive intermediates found during glucose hydrogenation reaction, the dehydration and other aldose-ketose isomerization processes were not taken into account in this work [27,33]. The real-time changes in the yield of those products and glucose conversion over 360 min of reaction are shown in Fig. 6 for the monometallic and bimetallic 1:1 formulations, along with the case of using a mixture of both monometallic catalysts, for comparison. It can be seen that in the first 40 min or so, glucose conversion curves with these different catalysts are all linearly correlated with the X axis time. Taking the experimental data of glucose conversion (x) presented in Fig. 6, and plotting Ln (1-x) over reaction time in the first 50 min, a linear fitting was indeed obtained in all cases (Figure S3). It should be noted that conversion (x) was determined at low conversion from the linear portion of reaction profiles, considering no mass-transport limitations and catalysts deactivation. So this pseudo-first-order dependence with respect to glucose was revealed under excess of H_2, which is consistent with previous reports [5,8]. In addition, the initial reaction rates with various catalysts was compared through the slopes of the profiles in Figure S3, giving the order $r_{Fe/CB} > r_{FeNi/CB} > r_{Fe/CB+Ni/CB} > r_{Ni/CB}$, where r is the initial reaction rate of glucose hydrogenation. So, Fe/CB is the most active catalyst in these conditions, followed by FeNi/CB, and the Ni/CB is the least active catalyst. The favoured reaction paths and corresponding product yields with each catalyst are discussed below.

The yield of the four key products and the conversion of glucose vs reaction time during glucose hydrogenation in the presence of the monometallic Fe/CB catalyst are illustrated in Fig. 6a. The conversion and various yields increased with time, while the rate of conversion decreased substantially over time, especially after 40 min, which may be attributed to insufficient amount of glucose remaining (drawback of batch reactor process) or catalyst deactivation. Additionally, a decrease in fructose yield was observed, probably due to its isomerization to glucose and hydrogenation to mannitol. Within 360 min, a total of 68 %

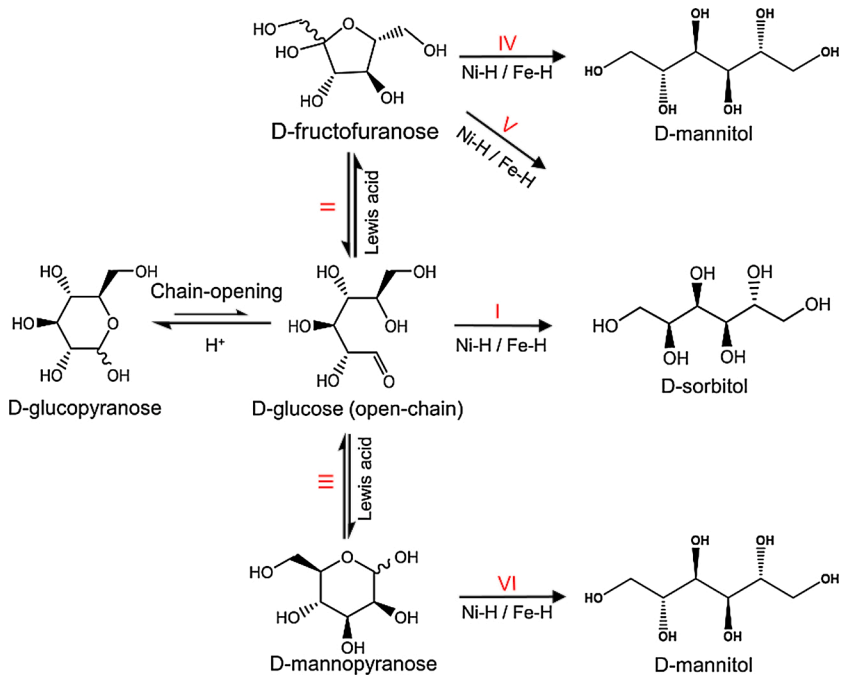


Fig. 5. Reaction network for D-glucose hydrogenation over Fe/CB, Ni/CB and Fe_xNi_y/CB catalysts at 140 °C, 30 bar H_2 and 1700 rpm stirring speed.

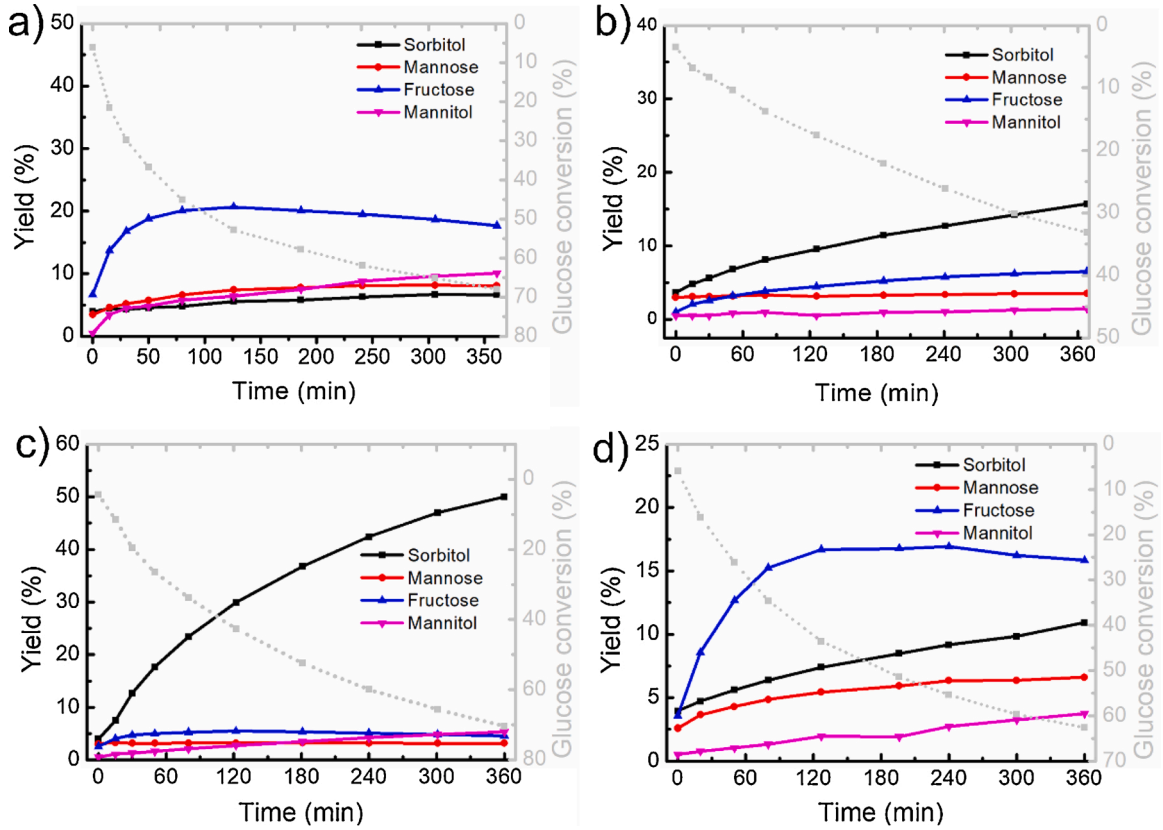


Fig. 6. Yield (left axis) of sorbitol (black), fructose (blue), mannose (red) and mannitol (pink) vs time and glucose conversion (right axis) vs time over Fe/CB (a), Ni/CB (b), FeNi/CB (c) and mixture of Fe/CB and Ni/CB (d) catalysts at 140 °C, 30 bar H_2, 1700 rpm and 360 min. Yield scales are different in each case to better highlight the differences for each species.

of the glucose was consumed in the reaction, giving 17.7 % yield in fructose, 10.1 % yield in mannitol, 8.1 % yield in mannose and 6.6 % yield in sorbitol, respectively. Thus, for the Fe/CB catalyst, isomerization of glucose to fructose is the most preferred reaction path, which is consistent with previous reports stating that Fe species are active sites for glucose isomerization [34]. In contrast, Ni/CB catalyst encourages a different reaction pathway (Fig. 6b). As described above, under the same conditions, the initial reaction rate on Ni/CB is lower than with Fe/CB,

thus only 33.1 % of glucose was transformed in the reaction, however sorbitol formed with a yield of 15.7 %, more than double that of Fe/CB catalyst. Additionally, lower yields of the undesired products were observed, fructose (6.5 % yield), mannose (3.5 % yield), and mannitol (1.5 % yield). Thus, while its activity is not as good as the Fe/CB catalyst, Ni/CB gave the desired sorbitol as the major product.

Interestingly, when Fe and Ni formed an alloy, the two metals promote each other, both driving the reaction via the sorbitol producing pathway and exhibiting higher activity. As a result, sorbitol is the dominate product with a yield of 50 % in 360 min, 3 times than that of Ni/CB (Fig. 6c). Moreover, isomerization of glucose to fructose seems to be depressed by Ni, and consequently, the yield of fructose is much lower than with the monometallic Fe/CB. The yields in mannose and mannitol remain similarly low. Glucose conversion with FeNi/CB also improved from 33.1 % to 70.5 % in comparison with Ni/CB. Thus, synergistic effects arise from alloying: the conversion of glucose and the yield in sorbitol are both highly improved, and simultaneously the isomerization of glucose is restricted. To further verify the presence of a synergistic effect in the alloy catalyst, a mechanical mixture of both Fe/CB and Ni/CB catalysts was used to catalyse glucose hydrogenation. It should be noted that in this case 30 mg of Fe/CB and 30 mg of Ni/CB were employed, instead of 60 mg in the previous cases, to keep the total metal quantity involved in the reaction constant. The glucose conversion and product yield results are shown in Fig. 6d. It is obvious that fructose is a major product with a similar line shape as for pure Fe/CB, which is attributed to the function of Fe/CB catalyst, and the sorbitol yield of 10.9 % is similar to the catalytic reaction with Ni/CB. In 360 min, 62.6 % of glucose was transformed in the reaction, which is also lower than of the conversion obtained with the FeNi/CB alloy. The hydrogenation results of the catalyst mixture indicate that its catalytic behaviour comes largely from the simple superposition of the results of the two single catalysts, that is, the mixing of two monometallic catalysts does not generate a synergistic effect like for the alloy. Electron rearrangement in the alloy may contribute to this synergistic effect. Since Fe atoms in FeNi/CB are more electropositive than Ni given their electron affinities, even under H_2 pressure, they can remain positively charged and act as adsorption sites for the open-chain glucose.

The results of real- time carbon balance are shown in Fig. 7, which was calculated using Eq. 4. It should be noted that C_b is underestimated when there are products obtained other than sorbitol, mannose, fructose and mannitol, because those unidentified minor by-products were not considered in this equation. All values of C_b with the four different catalysts decreased with prolonged reaction time, which may be attributed to increased by-products formation. As the C_b with Ni/CB and FeNi/CB catalysts were consistently higher than with Fe/CB and mixtures of Fe/CB and Ni/CB catalysts, it means that more side reactions occurred with Fe/CB and mixtures of the Fe/CB and Ni/CB catalysts than with the other two catalysts. These results support that, relative to Fe/CB and mixtures of Fe/CB and Ni/CB, synergistic effects in FeNi/CB reduce the occurrence of other side reactions over Fe metal surface, keeping the C_b above 92.6 %.

In order to investigate the principle of synergistic effects in Fe-Ni alloys with different compositions, the two other Fe_3Ni/CB and $FeNi_3$/CB catalysts were used to catalyse the glucose hydrogenation reaction, and their conversion and sorbitol selectivity results at 2 h are illustrated in Fig. 8. Carbon balance for all these cases was above 90 % except for Fe/CB where it is around 87 %. The Fe mass percentage in the alloy (x-axis) was directly correlated with conversion. As %Fe increased from 0 to 100 %, (from left to right) the conversion increased from 21.4 % to 52.8 %. This indicates that the activity of the alloy catalyst increases simply with the increment of Fe. However, the sorbitol selectivity decreases with Fe content, especially after 50 % Fe composition, while before it remains approximately unchanged. This is possibly due to the fact that in iron-rich samples, more Fe atoms are clustered within the alloy and do not feel the influence of Ni. Hence, these Fe atoms still exhibit the same electron distribution than in pure Fe samples, which favoured the isomerization reaction. This leads to lower selectivity of sorbitol. In a word, catalytic performance of Ni catalyst was promoted after adding Fe forming an alloy, but selectivity to sorbitol dropped seriously if the composition of iron exceed 50 %. Based on that, FeNi/CB with 1:1 atomic ratio appears to be the best compromise for achieving higher catalytic activity while maintaining high sorbitol selectivity. In this FeNi/CB alloy, the Fe and Ni atoms are supposed to be evenly distributed, which could maximize the activation of Ni, resulting in the optimal synergistic effect versus the other alloys.

A comparison of glucose conversion and sorbitol selectivity over different catalysts is shown in Table 3. With noble metal catalysts, especially for Ru, both conversion and selectivity reached around 100 % in a short reaction time and low metal usage. Catalysts based on monometallic Ni including the pure metal catalyst and supported catalysts showed relatively low glucose conversion (7–95 %). However, Ni-alloy catalysts have significantly improved catalytic activity. For example, with a NiCo catalyst and our FeNi catalyst, the conversion rate of glucose were both about 43 % in 2 h reaction and the selectivities were 41 % and 58 % respectively, which indicates the superiority of the alloy catalysts for improving the catalytic activity in this reaction.

3.3. Stability of catalysts

Catalyst structure, morphology, and surface chemical oxidation state before and after hydrogenation test were investigated to analyse the

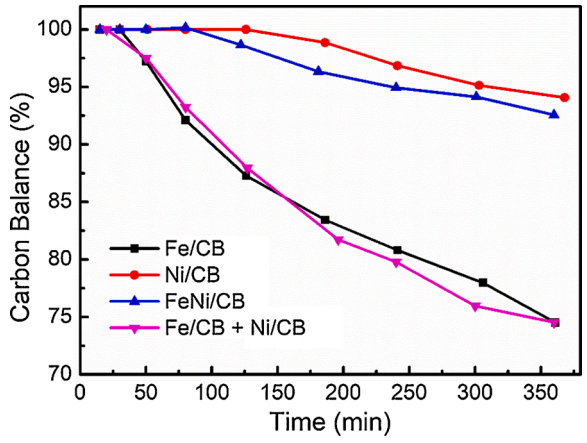


Fig. 7. Real-time carbon balance monitoring during glucose hydrogenation reaction over Fe/CB (black), Ni/CB (red), FeNi/CB (green) and mixture of Fe/CB and Ni/CB (pink) catalysts at 140 °C, 30 bar H_2, 1700 rpm and 360 min.

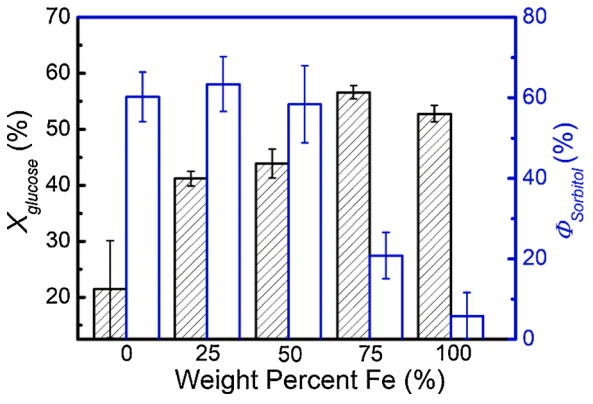


Fig. 8. Influence of composition of Fe-Ni/CB catalysts on glucose conversion ($X_{glucose}$) and sorbitol selectivity ($\Phi_{sorbitol}$). Reaction conditions: 60 mg catalyst, 0.5 g glucose, 100 ml H_2O, T = 140 °C, p (H_2) =30 bar, 120 min and stirring speed of 1700 rpm.

Table 3
Comparison of different noble and non-noble catalysts.

Catalyst	Catalyst amount (g)	Metal loading (%wt)	P (bar)	T (°C)	t (min)	Glucose conversion (%)	Sorbitol selectivity (%)	Ref.
$(RuO2)_{0.038}·(SiO2)_{0.962}$	0.5	6.3	20	120	60	~97	~100	[33]
Ru/C	>2	3.5–5.6	10–60	100–140	100–140	100	>98	[35]
Ru:Ni/MCM-48	NR	3	30	120	90	70	~100	[8]
Ru/MWNT	0.05	5	40	120	120	62.5	NR	[14]
Pt/SBA-15	0.2	1.5	40	140	120	13	63	[27]
Pt/AC	0.06	1–5	16	180	180	>95	>55	[36]
Ni/SiO_2	0.4	5–20	120	120	600	19–45	81–92	[7]
Ni/C	0.5	>4.81	120	120	600	7–10.5	0–23	[13]
Ni/NiO	0.05	100	50	100–150	NR	90–95	88–89	[15]
$Ni\text{-}B/SiO_2$	1	6.4	40	120	360	30	NR	[10]
NiCo/HZSM-5	0.1	15	30	120	120	~43	~41	[24]
FeNi/CB	0.06	16.6	30	140	120	43.9	58	

NR: no data were reported.

stability of those materials. They were labelled as *name*_Spent. The particle size of FeNi/CB_Spent was calculated by using the Debye–-Scherrer formula based on the XRD pattern (Figure S4) and visualized by TEM (Figure S5). XRD calculation results showed that the average size of the FeNi alloy particles increased from 9.0 nm to 17.1 nm after reaction. This particle growth can also be seen in the TEM images, since there were some bigger particles appearing in the spent catalysts (Figure S5b). XPS spectra revealed chemical state differences of Ni and Fe on the surface of fresh (Fig. 4c, d) and spent catalysts (Figure S6a, b). The red peaks correspond to metallic Ni (Ni^0) or Fe (Fe^0). It is obvious that the proportions of Ni^0 and Fe^0 in the catalyst diminished after hydrogenation test, but the remaining metallic surface Ni and Fe in FeNi/CB_Spent will still allow the chemisorption of H_2 and glucose. The metal leaching information was also a factor to take into account to determine the stability of catalysts, so Ni leaching weight loss percentage in Ni/CB and FeNi/CB catalysts after glucose hydrogenation are shown in Table S2. The leaching weight loss percentage was calculated by using the following formula:

$$Weight\ loss\ (\%) = \frac{m_{initial} - m_{real}}{m_{initial}} \times 100$$

$m_{initial}$ was the initial weight of Ni in fresh catalyst, m_{real} represents the determined content of Ni in spent catalysts. After the hydrogenation test, for the Ni/CB catalyst, around 10.8 % of Ni leached into the water medium, while on the contrary, only 6.5 % of Ni was leached away from FeNi/CB catalyst. So, the FeNi alloy catalyst could retard the leaching of Ni compared with the monometallic Ni catalyst.

The particle growth, partial oxidation, and leaching of Ni could lead to the loss of active sites, and deactivation of those catalysts. Here, we illustrated the catalytic performance with the fresh and spent catalysts in Fig. 9. For monometallic Ni catalyst, the spent catalyst gave still low glucose conversion and showed decreasing selectivity compared to the fresh one. For the alloy catalyst, both glucose conversion and sorbitol selectivity decreased when using the spent catalyst, but its glucose conversion was still 3 times higher than the fresh monometallic Ni catalyst (Ni/CB), which testified that Fe in the alloy could promote Ni active sites to maintain high catalytic activity during recycling. In summary, thanks to the synergistic effect, the alloy catalyst can preserve metallic active sites of Ni and reduce its leaching, thereby maintaining better stability, compared to monometallic nickel catalyst.

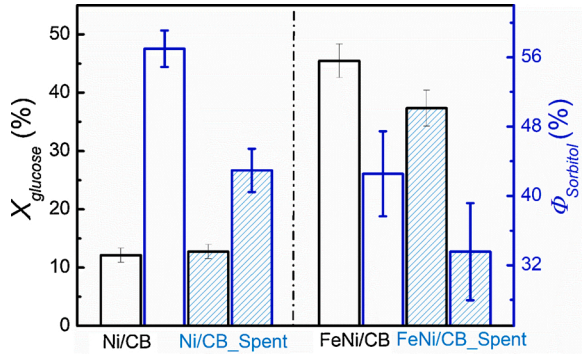


Fig. 9. Glucose conversion ($X_{glucose}$) and sorbitol selectivity ($\Phi_{sorbitol}$) over fresh and spent catalysts. Reaction conditions: 60 mg catalyst, 0.5 g glucose, 100 mL H_2O, T = 120 °C, p (H_2) =30 bar, 120 min and stirring speed of 1700 rpm.

4. Conclusions

Aiming at investigating the synergistic effect in alloy Fe-Ni catalysts during glucose hydrogenation, monometallic Fe, Ni and Fe-Ni alloy catalysts supported by CB were synthesised through a sol-gel method. XRD results demonstrated that an alloy phase was formed in the bimetallic catalysts. HAADF-TEM images and EDS analysis evidenced that the size distribution and composition of the nanoparticles were uniform. Fe and Ni in the alloy form were found to be less prone to oxidation than monometallic Fe and Ni through XPS analysis, so metallic Fe and Ni sites remain at the surface of the bimetallic catalysts, contributing to the splitting of hydrogen necessary for the catalytic transformation.

By analysing the hydrogenation reaction of glucose over monometallic and alloy catalysts, it was found that Fe and Ni favour different reaction pathways and that synergistic effects were present with the FeNi alloy catalysts. With the Fe/CB catalyst, 68 % of glucose was transformed in the reaction, with fructose as the major product, obtained in 17.7 % yield, while only 6.6 % of sorbitol was produced. For the Ni/CB catalyst, in which glucose to sorbitol is the dominating pathway, a higher percentage of sorbitol (15.7 %) was obtained but overall glucose conversion was lower (33.1 %). Interestingly, the glucose conversion and sorbitol productivity were enhanced to a great extent when Fe and Ni formed an alloy, with a glucose conversion of 70.4 % and sorbitol yield of 50 %. This synergistic effect cannot be observed with a simple mixture of Fe/CB and Ni/CB catalysts, as electronic effects only appears in alloys. By comparing catalytic performance using Fe-Ni alloys with different compositions, FeNi/CB with an atomic ratio of 1:1 was identified as the best catalyst for efficient hydrogenation of glucose to sorbitol. Particle growth, surface oxidation and leaching caused the deactivation of Ni - based catalyst, but the FeNi alloy catalyst exhibited obvious advantages over monometallic the Ni catalyst in terms of stability.

CRediT authorship contribution statement

Yang Fu: Methodology, Validation, Investigation, Writing - original draft, Visualization. **Lipeng Ding:** Investigation. **Michael L. Singleton:** Supervision, Writing - review & editing, Project administration. **Hosni Idrissi:** Investigation, Writing - review & editing. **Sophie Hermans:** Conceptualization, Methodology, Resources, Writing - review & editing, Supervision, Project administration, Funding acquisition.

Declaration of Competing Interest

The authors declare that they have no known competing financial interests or personal relationships that could have appeared to influence the work reported in this paper.

Acknowledgements

The authors gratefully acknowledge Jean-François Statsyns for technical assistance, François Devred for XRD analyses and IMERYS GRAPHITE & CARBON (Switzerland) firm for generous donation of carbon black. Y. F. thanks Pierre Eloy for helpful discussion about XPS analysis and China Scholarship Council (CSC) for the financial support. H.I. and S.H are mandated by the Belgian National Fund for Scientific Research (FSR-FNRS).

Appendix A. Supplementary data

Supplementary material related to this article can be found, in the online version, at doi:https://doi.org/10.1016/j.apcatb.2021.119997.

References

[1] T. Werpy, G. Petersen, Top Value Added Chemicals From Biomass: Volume I–results of Screening for Potential Candidates From Sugars and Synthesis Gas, National Renewable Energy Lab., Golden, CO (US), 2004.
[2] S. Carlier, J. Gripekoven, M. Philippo, S. Hermans, Ru on N-doped carbon supports for the direct hydrogenation of cellobiose into sorbitol, Appl. Catal. B 282 (2021) 119515, https://doi.org/10.1016/j.apcatb.2020.119515.
[3] M. Abdel Akher, J. Ghali, M.S. Raouf, M. Roushdi, Factors Affecting the Catalytic Hydrogenation of D-Glucose. Part I. Effect of Type of Catalyst and Concentrations of both Glucose and Catalyst, Starch - Stärke 26 (1974) 307–312, https://doi.org/10.1002/star.19740260904.
[4] P.H. Brahme, M.U. Pai, G. Narsimhan, Hydrogenation of glucose to polyhydric, Brit. Chem. Eng. 9 (1964) 684–687.
[5] J. Wisnlak, R. Simon, Hydrogenation of glucose, fructose, and their mixtures, Ind. Eng. Chem. Prod. Res. Dev. 18 (1979) 50–57, https://doi.org/10.1021/i360069a011.
[6] B.J. Arena, Deactivation of ruthenium catalysts in continuous glucose hydrogenation, Appl. Catal. A 87 (1992) 219–229, https://doi.org/10.1016/0926-860X(92)80057-J.
[7] S. Schimpf, C. Louis, P. Claus, Ni/SiO_2 catalysts prepared with ethylenediamine nickel precursors: influence of the pretreatment on the catalytic properties in glucose hydrogenation, Appl. Catal. A 318 (2007) 45–53, https://doi.org/10.1016/j.apcata.2006.10.034.
[8] A. Romero, A. Nieto-Márquez, E. Alonso, Bimetallic Ru:Ni/MCM-48 catalysts for the effective hydrogenation of D-glucose into sorbitol, Appl. Catal. A 529 (2017) 49–59, https://doi.org/10.1016/j.apcata.2016.10.018.
[9] G. Schmid, Large clusters and colloids. Metals in the embryonic state, Chem. Rev. 92 (1992) 1709–1727, https://doi.org/10.1021/cr00016a002.
[10] H. Li, H. Li, J.F. Deng, Glucose hydrogenation over Ni-B/SiO_2 amorphous alloy catalyst and the promoting effect of metal dopants, Catal. Today 74 (2002) 53–63, https://doi.org/10.1016/S0920-5861(01)00530-2.
[11] S. Van Den Bosch, T. Renders, S. Kennis, S.F. Koelewijn, G. Van Den Bossche, T. Vangeel, A. Deneyer, D. Depuydt, C.M. Courtin, J.M. Thevelein, W. Schutyser, B. F. Sels, Integrating lignin valorization and bio-ethanol production: on the role of Ni-Al2O3 catalyst pellets during lignin-first fractionation, Green Chem. 19 (2017) 3313–3326, https://doi.org/10.1039/c7gc01324h.
[12] A. Negoi, K. Triantafyllidis, V.I. Parvulescu, S.M. Coman, The hydrolytic hydrogenation of cellulose to sorbitol over M (Ru, Ir, Pd, Rh)-BEA-zeolite catalysts, Catal. Today 223 (2014) 122–128, https://doi.org/10.1016/j.cattod.2013.07.007.
[13] B. Kusserow, S. Schimpf, P. Claus, Hydrogenation of glucose to sorbitol over nickel and ruthenium catalysts, Adv. Synth. Catal. 345 (2003) 289–299, https://doi.org/10.1002/adsc.200390024.
[14] J. Pan, J. Li, C. Wang, Z. Yang, Multi-wall carbon nanotubes supported ruthenium for glucose hydrogenation to sorbitol, React. Kinet. Catal. Lett. 90 (2007) 233–242, https://doi.org/10.1007/s11144-007-4989-4.
[15] H. Singh, A. Rai, R. Yadav, A.K. Sinha, Glucose hydrogenation to sorbitol over unsupported mesoporous Ni/NiO catalyst, Mol. Catal. 451 (2018) 186–191, https://doi.org/10.1016/j.mcat.2018.01.010.
[16] P.J. Cerino, G. Fleche, P. Gallezot, J.P. Salome, Activity and stability of promoted Raney-Nickel catalysts in glucose hydrogenation, in: M. Guisnet, J. Barrault, C. Bouchoule, D. Duprez, G. Pérot, R. Maurel, C. Montassier (Eds.), Studies in Surface Science and Catalysis, Elsevier, 1991, pp. 231–236.
[17] J. Court, J.P. Damon, J. Masson, P. Wierzchowski, Hydrogenation of glucose with bimetallic catalysts (NiM) of Raney type, in: M. Guisnet, J. Barrault, C. Bouchoule, D. Duprez, C. Montassier, G. Pérot (Eds.), Heterogeneous Catalysis and Fine Chemicals, Proceedings of an International Symposium, Elsevier, 1988, pp. 189–196.
[18] P. Gallezot, P.J. Cerino, B. Blanc, G. Flèche, P. Fuertes, Glucose hydrogenation on promoted raney-nickel catalysts, J. Catal. 146 (1994) 93–102, https://doi.org/10.1016/0021-9517(94)90012-4.
[19] F.M. Mederos-Henry, B.P. Pichon, M.M. Dîrtu, Y. Garcia, A. Delcorte, C. Bailly, I. Huynen, S. Hermans, Highly efficient wideband microwave absorbers based on zero-valent Fe@γ-Fe_2O_3 and Fe/Co/Ni carbon-protected alloy nanoparticles supported on reduced graphene oxide, Nanomaterials 9 (2019) 1196, https://doi.org/10.3390/nano9091196.
[20] K. Hadjiivanov, M. Mihaylov, D. Klissurski, P. Stefanov, N. Abadjieva, E. Vassileva, L. Mintchev, Characterization of Ni/SiO_2 catalysts prepared by successive deposition and reduction of Ni^{2+} ions, J. Catal. 185 (1999) 314–323, https://doi.org/10.1006/jcat.1999.2521.
[21] A. Lutts, P.M. Gielen, The order-disorder transformation in $FeNi_3$, Phys. Status Solidi B 41 (1970) K81–K84, https://doi.org/10.1002/pssb.19700410169.
[22] M.C. Biesinger, B.P. Payne, A.P. Grosvenor, L.W.M. Lau, A.R. Gerson, R.S.C. Smart, Resolving surface chemical states in XPS analysis of first row transition metals, oxides and hydroxides: Cr, Mn, Fe, Co and Ni, Appl. Surf. Sci. 257 (2011) 2717–2730, https://doi.org/10.1016/j.apsusc.2010.10.051.
[23] F.U. Hillebrecht, J.C. Fuggle, P.A. Bennett, Z. Zołnierek, C. Freiburg, Electronic structure of Ni and Pd alloys. II. X-ray photoelectron core-level spectra, Phys. Rev. B 27 (1983) 2179–2193, https://doi.org/10.1103/PhysRevB.27.2179.
[24] B. Zada, L. Yan, Y. Fu, Effective conversion of cellobiose and glucose to sorbitol using non-noble bimetallic NiCo/HZSM-5 catalyst, Sci. China Chem. 61 (2018) 1167–1174, https://doi.org/10.1007/s11426-018-9321-0.
[25] M. Makkee, A.P.G. Kieboom, H. Van Bekkum, Hydrogenation of d-fructose and d-fructose/d-glucose mixtures, Carbohydr. Res. 138 (1985) 225–236, https://doi.org/10.1016/0008-6215(85)85106-5.
[26] J.M. Los, L.B. Simpson, K. Wiesner, The kinetics of mutarotation of D-Glucose with consideration of an intermediate free-aldehyde form, J. Am. Chem. Soc. 78 (1956) 1564–1568, https://doi.org/10.1021/ja01589a017.
[27] X. Zhang, L.J. Durndell, M.A. Isaacs, C.M.A. Parlett, A.F. Lee, K. Wilson, Platinum-Catalyzed Aqueous-Phase Hydrogenation of d-Glucose to d-Sorbitol, ACS Catal. 6 (2016) 7409–7417, https://doi.org/10.1021/acscatal.6b02369.
[28] R.W. Nagorski, J.P. Richard, Mechanistic imperatives for aldose−Ketose isomerization in water: specific, general base- and metal ion-catalyzed isomerization of Glyceraldehyde with proton and hydride transfer, J. Am. Chem. Soc. 123 (2001) 794–802, https://doi.org/10.1021/ja003433a.
[29] S.S. Chen, D.C.W. Tsang, J.-P. Tessonnier, Comparative investigation of homogeneous and heterogeneous Brønsted base catalysts for the isomerization of glucose to fructose in aqueous media, Appl. Catal. B 261 (2020) 118126, https://doi.org/10.1016/j.apcatb.2019.118126.
[30] Y. Román-Leshkov, M. Moliner, J.A. Labinger, M.E. Davis, Mechanism of glucose isomerization using a solid lewis acid catalyst in water, Angew. Chem., Int. Ed. 49 (2010) 8954–8957, https://doi.org/10.1002/anie.201004689.
[31] R. Bermejo-Deval, M. Orazov, R. Gounder, S.-J. Hwang, M.E. Davis, Active sites in Sn-Beta for glucose isomerization to fructose and epimerization to mannose, ACS Catal. 4 (2014) 2288–2297, https://doi.org/10.1021/cs500466j.
[32] M. Moliner, Y. Román-Leshkov, M.E. Davis, Tin-containing zeolites are highly active catalysts for the isomerization of glucose in water, Proc. Natl. Acad. Sci. 107 (2010) 6164–6168, https://doi.org/10.1073/pnas.1002358107.
[33] S. Esposito, B. Silvestri, V. Russo, B. Bonelli, M. Manzoli, F.A. Deorsola, A. Vergara, A. Aronne, M. Di Serio, Self-activating catalyst for glucose hydrogenation in the aqueous phase under mild conditions, ACS Catal. 9 (2019) 3426–3436, https://doi.org/10.1021/acscatal.8b04710.
[34] S. Xu, L. Zhang, K. Xiao, H. Xia, Isomerization of glucose into fructose by environmentally friendly Fe/β zeolite catalysts, Carbohydr. Res. 446-447 (2017) 48–51, https://doi.org/10.1016/j.carres.2017.05.006.
[35] B.W. Hoffer, E. Crezee, P.R.M. Mooijman, A.D. van Langeveld, F. Kapteijn, J. A. Moulijn, Carbon supported Ru catalysts as promising alternative for Raney-type Ni in the selective hydrogenation of d-glucose, Catal. Today 79-80 (2003) 35–41, https://doi.org/10.1016/S0920-5861(03)00040-3.
[36] P.A. Lazaridis, S. Karakoulia, A. Delimitis, S.M. Coman, V.I. Parvulescu, K. S. Triantafyllidis, d-Glucose hydrogenation/hydrogenolysis reactions on noble metal (Ru, Pt)/activated carbon supported catalysts, Catal. Today 257 (2015) 281–290, https://doi.org/10.1016/j.cattod.2014.12.006.